

Dynamics of immersed molecules in superfluids

Michael J. Quist and Veit Elser

Department of Physics, Cornell University, Ithaca, New York 14850

(Dated: April 27, 2019)

The dynamics of a molecule immersed in a superfluid medium are considered. Results are derived using a classical hydrodynamic approach followed by canonical quantization. The classical model, a rigid body immersed in incompressible fluid, permits a thorough analysis; its effective Hamiltonian generalizes the usual rigid-rotor Hamiltonian. In contrast to the free rigid rotor, the immersed body is shown to have chaotic dynamics. Quantization of the classical model leads to new and experimentally verifiable features. It is shown, for instance, that chiral molecules can behave as “quantum propellers”: the rotational-translational coupling induced by the superfluid leads to a nonzero linear momentum in the ground state. Hydrogen peroxide is a strong candidate for experimental detection of this effect. The signature is a characteristic splitting of rotational absorption lines. The $1_{01} \rightarrow 1_{10}$ line in hydrogen peroxide, for example, is predicted to split into three lines separated by as much as 0.05 cm^{-1} , or five times the experimental linewidth.

I. INTRODUCTION

The dynamics of a molecule moving within a superfluid medium are not expected to be too different from its dynamics in vacuum. Like the vacuum, an unbounded fluid is homogeneous and invariant with respect to continuous translations and rotations. Moreover, in the exotic case of superfluids, the very low level of excitation achieved at low temperatures implies that there is a vanishing set of modes with which the immersed molecule can interact. These expectations are borne out in the spectroscopy of single impurity molecules in ^4He nanodroplets, where the superfluid medium has little effect on the rotational spectrum beyond modifying the molecular moments of inertia.^{1,2,3}

On the other hand, a low temperature superfluid medium is distinct from the nonrelativistic vacuum in that it lacks a basic symmetry: Galilean invariance. The superfluid condensate defines a preferred rest frame, an “ether” relative to which molecular velocities should be measured. This implies, in particular, that the energy-momentum relationship of molecules immersed in superfluids can deviate from a parabolic form. Of more interest spectroscopically, the presence of a preferred rest frame also gives rise to the possibility of rotational-translational couplings that are strictly forbidden in an environment with Galilean invariance. Evidence of such couplings would provide one of the most direct experimental signatures of the superfluid medium.

This paper develops a simple and general theoretical framework for the rigid-body dynamics of a molecule immersed in a bosonic superfluid. The classical analysis of an immersed body, presented in Section II, shows that an incompressible fluid medium adds 11 parameters to the usual 4 parameters characterizing a free rigid body. As a result, an immersed body is typically chaotic. The classical model is quantized in Section III, and the quantum Hamiltonian is discussed. The most interesting new feature is a term of the form $\mathbf{p} \cdot \mathbf{J}$ which directly couples the linear momentum and spin angular momentum of the molecule. This coupling requires chirality in the molecule, and corresponds intuitively to the action of a propeller. It fully lifts the usual $(2J + 1)$ -fold degeneracy of rigid-rotor states with angular momentum J , providing a clear spectroscopic signature of the superfluid-induced rotational-translational coupling. An unusual consequence is that the ground state acquires nonzero linear momentum. In Section IV, the magnitude of the rotational-translational coupling is estimated for the chiral molecules HOOH and FOOF. The predicted splitting of rotational absorption lines, at least for HOOH, is well above the resolution of current experiments. Finally, in Section V, the results are discussed in the context of related work.

II. CLASSICAL MECHANICS OF AN IMMERSED RIGID BODY

We consider a rigid body immersed in unbounded, incompressible fluid of density ρ_f . The body occupies a bounded, simply-connected volume V from which the fluid is excluded; the surface of this volume is denoted by ∂V . The velocity of the fluid is described by a potential $\phi(\mathbf{x})$, such that $\mathbf{v}_f = \nabla\phi$, which satisfies $\nabla^2\phi = 0$ inside the fluid volume and $|\nabla\phi(\mathbf{x})| \rightarrow 0$ as $|\mathbf{x}| \rightarrow \infty$. On the moving surface ∂V , the fluid velocity also must satisfy $(\mathbf{v}_f - \mathbf{v}_s) \cdot \mathbf{n} = 0$, where \mathbf{n} is the surface normal and \mathbf{v}_s is the surface velocity.

We choose an origin and coordinate axes fixed in the body; this defines the body frame. The origin of the body frame is at \mathbf{y} in the lab frame, and the body axes are rotated by $\hat{\mathcal{R}}$ from the lab axes. The three components of \mathbf{y} and the three Euler angles needed to parametrize the matrix $\hat{\mathcal{R}}$ completely specify the position of the body. When $\mathbf{y} = \mathbf{0}$ and $\hat{\mathcal{R}} = \hat{\mathbb{I}}$, the body and lab frames coincide, and the body is said to be in the reference position. Let E_t be

the Euclidean transformation which moves the body from the reference position to its position at time t . Explicitly,

$$E_t : \mathbf{x} \mapsto \mathbf{y}(t) + \hat{\mathcal{R}}(t)\mathbf{x}. \quad (1)$$

The time-dependence of V is simply $V_t = E_t V_0$, where V_0 is a fixed volume; similarly, $\partial V_t = E_t \partial V_0$. The lab-frame velocity of a point $E_t \mathbf{x}$, which is fixed in the body, is

$$\frac{d}{dt}(E_t \mathbf{x}) = \dot{\mathbf{y}} + \boldsymbol{\omega} \times (\hat{\mathcal{R}} \mathbf{x}), \quad (2)$$

where $\boldsymbol{\omega}$ is the body's angular velocity. The velocity potential in the body frame, $\phi'(\mathbf{x}) \equiv \phi(E_t \mathbf{x})$, satisfies fairly simple equations: $\nabla^2 \phi' = 0$ outside V_0 , $|\nabla \phi'(\mathbf{x})| \rightarrow 0$ as $|\mathbf{x}| \rightarrow \infty$, and

$$\begin{aligned} \nabla \phi'(\mathbf{x}) \cdot \mathbf{n} &= \left(\hat{\mathcal{R}}^T \mathbf{v}_s(E_t \mathbf{x}) \right) \cdot \mathbf{n} \\ &= \left(\hat{\mathcal{R}}^T \dot{\mathbf{y}} + (\hat{\mathcal{R}}^T \boldsymbol{\omega}) \times \mathbf{x} \right) \cdot \mathbf{n} \end{aligned} \quad (3)$$

for \mathbf{x} on the fixed surface ∂V_0 , where the surface velocity was calculated using Eq. (2). Indeed, the equations for ϕ' are linear, with inhomogeneous boundary conditions linear in $\hat{\mathcal{R}}^T \dot{\mathbf{y}}$ and $\hat{\mathcal{R}}^T \boldsymbol{\omega}$. The velocity potential can therefore be expressed as a linear combination,

$$\phi'(\mathbf{x}) = (\hat{\mathcal{R}}^T \dot{\mathbf{y}})_\mu \psi_\mu(\mathbf{x}) + (\hat{\mathcal{R}}^T \boldsymbol{\omega})_\mu \chi_\mu(\mathbf{x}), \quad (4)$$

where the harmonic functions ψ_μ and χ_μ satisfy

$$\nabla \psi_\mu(\mathbf{x}) \cdot \mathbf{n} = \mathbf{e}_\mu \cdot \mathbf{n}, \quad (5a)$$

$$\nabla \chi_\mu(\mathbf{x}) \cdot \mathbf{n} = (\mathbf{e}_\mu \times \mathbf{x}) \cdot \mathbf{n} \quad (5b)$$

on ∂V_0 . These six functions characterize the fluid response to the six independent motions of the body; they depend only on the shape of ∂V_0 .

For a free rigid body, the Lagrangian is just the kinetic energy. When the body is immersed, this is augmented by the kinetic energy of the fluid:

$$\begin{aligned} \delta L &= \int_{V_0^c} d^3 x \frac{1}{2} \rho_f |\nabla \phi(\mathbf{x})|^2 \\ &= \int_{V_0^c} d^3 x \frac{1}{2} \rho_f |\nabla \phi'(\mathbf{x})|^2, \end{aligned} \quad (6)$$

where the second integral is over the fluid volume V_0^c , the complement of the body volume V_0 . This is easy to evaluate using Eq. (4). The total Lagrangian, including the fluid contribution [Eq. (6)], then has the form

$$L = \frac{1}{2} \begin{pmatrix} \dot{\mathbf{y}}^T \hat{\mathcal{R}} & \boldsymbol{\omega}^T \hat{\mathcal{R}} \end{pmatrix} \begin{pmatrix} \hat{M} & \hat{G} \\ \hat{G}^T & \hat{I} \end{pmatrix} \begin{pmatrix} \hat{\mathcal{R}}^T \dot{\mathbf{y}} \\ \hat{\mathcal{R}}^T \boldsymbol{\omega} \end{pmatrix}. \quad (7)$$

The mass tensor \hat{M} , the rotational-translational coupling tensor \hat{G} , and the inertia tensor \hat{I} can each be expressed as a sum of rigid-body and fluid tensors: $\hat{M} = \hat{M}^{(0)} + \delta \hat{M}$ and so on.

The rigid-body tensors are

$$M_{\mu\nu}^{(0)} = \int d^3 x \rho(\mathbf{x}) \delta_{\mu\nu}, \quad (8a)$$

$$G_{\mu\nu}^{(0)} = \int d^3 x \rho(\mathbf{x}) \epsilon_{\mu\nu\lambda} x_\lambda, \quad (8b)$$

$$I_{\mu\nu}^{(0)} = \int d^3 x \rho(\mathbf{x}) (|\mathbf{x}|^2 \delta_{\mu\nu} - x_\mu x_\nu), \quad (8c)$$

where $\rho(\mathbf{x})$ is the body-frame mass density of the body. The expressions for $\hat{M}^{(0)}$ and $\hat{I}^{(0)}$ are the usual ones, and $\hat{G}^{(0)}$ is typically made to vanish by choosing the body's center of mass as the origin of the body frame. The rigid-body Lagrangian then takes the familiar form

$$L^{(0)} = \frac{1}{2} \dot{\mathbf{y}}^T \hat{M}^{(0)} \dot{\mathbf{y}} + \frac{1}{2} \boldsymbol{\omega}^T \hat{\mathcal{R}} \hat{I}^{(0)} \hat{\mathcal{R}}^T \boldsymbol{\omega}. \quad (9)$$

The fluid tensors are

$$\delta M_{\mu\nu} = \int_{V_0^c} d^3x \rho_f \nabla \psi_\mu(\mathbf{x}) \cdot \nabla \psi_\nu(\mathbf{x}), \quad (10a)$$

$$\delta G_{\mu\nu} = \int_{V_0^c} d^3x \rho_f \nabla \psi_\mu(\mathbf{x}) \cdot \nabla \chi_\nu(\mathbf{x}), \quad (10b)$$

$$\delta I_{\mu\nu} = \int_{V_0^c} d^3x \rho_f \nabla \chi_\mu(\mathbf{x}) \cdot \nabla \chi_\nu(\mathbf{x}). \quad (10c)$$

Note that the mass and inertia tensors \hat{M} and \hat{I} are symmetric, while the rotational-translational coupling \hat{G} has no obvious symmetry. In the most general case there are $6 + 6 + 9 = 21$ parameters in the Lagrangian. We can place the body origin at a conveniently chosen point in the body, reducing this to 18. We can then rotate the body axes with respect to the body, leaving 15. By comparison, the free rigid rotor has 4 parameters.

The classical Hamiltonian follows from the Lagrangian [Eq. (7)]:

$$\mathcal{H} = \frac{1}{2} (\mathbf{p}^T \hat{\mathcal{R}} \quad \mathbf{J}^T \hat{\mathcal{R}}) \begin{pmatrix} \hat{M} & \hat{G} \\ \hat{G}^T & \hat{I} \end{pmatrix}^{-1} \begin{pmatrix} \hat{\mathcal{R}}^T \mathbf{p} \\ \hat{\mathcal{R}}^T \mathbf{J} \end{pmatrix}, \quad (11)$$

where \mathbf{p} is the linear momentum, canonically conjugate to \mathbf{y} , and \mathbf{J} is the (spin) angular momentum in the lab frame. The components of \mathbf{J} have Poisson brackets $[J_\mu, J_\nu]_{\text{cl}} = \epsilon_{\mu\nu\lambda} J_\lambda$. It is convenient also to work with $\mathbf{J}' = \hat{\mathcal{R}}^T \mathbf{J}$ and $\mathbf{p}' = \hat{\mathcal{R}}^T \mathbf{p}$, the angular and linear momenta in the body frame, in terms of which the Hamiltonian is particularly simple. These variables have Poisson brackets $[J'_\mu, J'_\nu]_{\text{cl}} = -\epsilon_{\mu\nu\lambda} J'_\lambda$ and $[J'_\mu, p'_\nu]_{\text{cl}} = -\epsilon_{\mu\nu\lambda} p'_\lambda$. The classical Poisson brackets relate to the quantum commutators in the usual way, as $[A, B] = i[A, B]_{\text{cl}}$.

To express Eq. (11) in a form more amenable to quantization, we first define new tensors $\hat{\alpha}$, $\hat{\beta}$, and $\hat{\gamma}$ through

$$\begin{pmatrix} \hat{\alpha} & \hat{\beta} \\ \hat{\beta}^T & \hat{\gamma} \end{pmatrix} \equiv \begin{pmatrix} \hat{M} & \hat{G} \\ \hat{G}^T & \hat{I} \end{pmatrix}^{-1}. \quad (12)$$

In the following section it is shown that $\hat{\beta}$ must be symmetric in order to avoid complication when quantizing the model. We can symmetrize $\hat{\beta}$ by choosing the body frame's origin correctly. It is not hard to see that the tensors $\hat{\alpha}$, $\hat{\beta}$, and $\hat{\gamma}$ transform in a particular way when the body origin is translated within the body; this can be used to find the appropriate choice of origin. For a free rigid body, the body's center of mass is the correct choice, but this is not true in general. After the body origin is fixed, rotation of the body axes can be used to diagonalize $\hat{\gamma}$, leaving it in the form $\hat{\gamma} = \text{diag}(2A, 2B, 2C)$. Note that A , B , and C are *effective* rotational constants, shifted from their rigid-body values by the body's interaction with the fluid. Finally, the symmetric matrices $\hat{\alpha}$ and $\hat{\beta}$ can be broken down into their scalar and rank-2 spherical tensor components:

$$\hat{\alpha} = \alpha_0^{(0)} \hat{\mathbb{1}} + \sum_{q=-2}^2 \alpha_q^{(2)} \hat{\mathcal{M}}_q^{(2)}, \quad (13)$$

and analogously for $\hat{\beta}$, where

$$\hat{\mathcal{M}}_0^{(2)} = \frac{1}{\sqrt{6}} \begin{pmatrix} -1 & & \\ & -1 & \\ & & 2 \end{pmatrix}, \quad \hat{\mathcal{M}}_{\pm 1}^{(2)} = -\frac{1}{2} \begin{pmatrix} 0 & 0 & \pm 1 \\ 0 & 0 & i \\ \pm 1 & i & 0 \end{pmatrix}, \quad \hat{\mathcal{M}}_{\pm 2}^{(2)} = \frac{1}{2} \begin{pmatrix} 1 & \pm i & 0 \\ \pm i & -1 & 0 \\ 0 & 0 & 0 \end{pmatrix}. \quad (14)$$

These matrices are defined to have nice rotational properties; in particular,

$$\hat{\mathcal{R}} \hat{\mathcal{M}}_q^{(2)} \hat{\mathcal{R}}^T = \sum_p \hat{\mathcal{M}}_p^{(2)} \mathcal{D}_{pq}^{(2)}, \quad (15)$$

where the $\mathcal{D}_{pq}^{(2)}$ are rotation matrices, given by known functions of the Euler angles.⁴ The Hamiltonian then has the form

$$\mathcal{H} = \frac{1}{2} \alpha_0^{(0)} p^2 + \beta_0^{(0)} \mathbf{p} \cdot \mathbf{J} + \mathcal{H}_{rr}(A, B, C) + \sum_q \frac{1}{2} \alpha_q^{(2)} \Pi_q^{(2)} + \sum_q \beta_q^{(2)} \Theta_q^{(2)}, \quad (16)$$

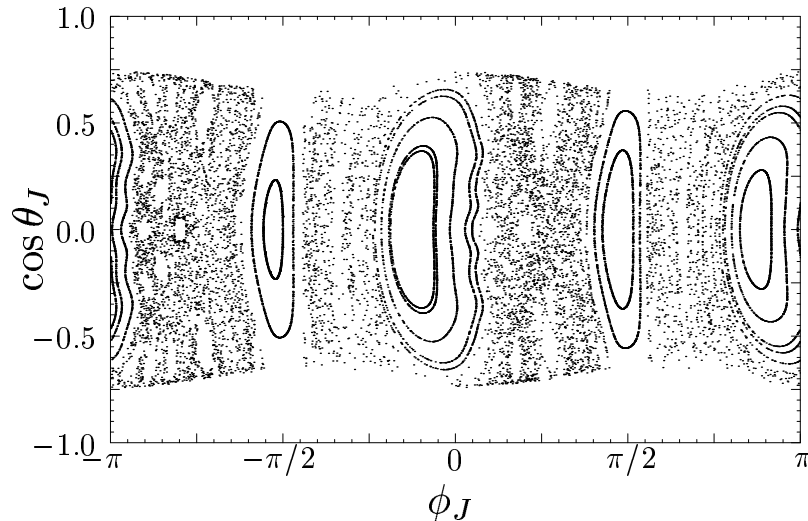


FIG. 1: Poincaré section of the reduced phase space of an immersed body, showing both chaotic and quasi-integrable regions.

where \mathcal{H}_{rr} is the rigid rotor Hamiltonian,

$$\mathcal{H}_{rr}(A, B, C) = AJ_x'^2 + BJ_y'^2 + CJ_z'^2, \quad (17)$$

and $\Pi^{(2)}$ and $\Theta^{(2)}$ are spherical tensors of rank 2, with components

$$\Pi_q^{(2)} = (\mathbf{p}')^T \hat{\mathcal{M}}_q^{(2)} \mathbf{p}'; \quad \Theta_q^{(2)} = (\mathbf{p}')^T \hat{\mathcal{M}}_q^{(2)} \mathbf{J}'. \quad (18)$$

More precisely, $\Pi^{(2)}$ and $\Theta^{(2)}$ transform as spherical tensors of rank 2 under rotations generated by $-\mathbf{J}'$.

Before proceeding to the quantum case, we consider the classical dynamics of the model. The Lagrangian is invariant under arbitrary translations ($\mathbf{y} \mapsto \mathbf{y} + \mathbf{a}$) and system rotations ($\mathbf{y} \mapsto \hat{\mathcal{O}}\mathbf{y}$, $\hat{\mathcal{R}} \mapsto \hat{\mathcal{O}}\hat{\mathcal{R}}$), but not under body rotations ($\hat{\mathcal{R}} \mapsto \hat{\mathcal{O}}\hat{\mathcal{R}}$) alone. Therefore \mathbf{p} and the total (spin plus orbital) angular momentum $\mathbf{J} + \mathbf{y} \times \mathbf{p}$ are constants of the motion, but \mathbf{J} is not, in contrast to the free rigid rotor. We can use these symmetries to simplify the system. Four constants of the motion, which have vanishing Poisson brackets with \mathcal{H} and with each other, are $\mathbf{p} \cdot \mathbf{J}$ and the components of \mathbf{p} . By fixing these constants and eliminating the coordinates which are conjugate to them (the components of \mathbf{y} and one of the three Euler angles), we restrict the Hamiltonian to a reduced phase space; the equations of motion for the remaining degrees of freedom are unchanged by the reduction. In this case, the original six degrees of freedom are reduced to two, so the reduced phase space is four-dimensional. It can be parametrized by the directions of \mathbf{p}' and \mathbf{J}' , expressed in polar coordinates by the four angles $(\theta_p, \phi_p, \theta_J, \phi_J)$. The energy shells of the reduced phase space (i.e., the level sets of \mathcal{H}) are three-dimensional.

The integrability of a Hamiltonian system with two degrees of freedom can be ascertained using a Poincaré section, essentially by inspection. To illustrate that the immersed rigid body is generally chaotic, we display a Poincaré section of the reduced phase space in Fig. 1. The figure was generated by repeatedly integrating the equations of motion, starting at many different points within the $\mathcal{H} = 2$ energy shell, and plotting the point $(\phi_J, \cos \theta_J)$ each time a trajectory crossed the plane $\theta_p = \pi/2$. The Hamiltonian parameters were $\hat{\alpha} = \hat{\mathbb{1}}$, $\hat{\beta} = \text{diag}(1, 1, -2)$, and $\hat{\gamma} = \text{diag}(1, 2, \sqrt{5})$; the conserved quantities were set to $\mathbf{p} \cdot \mathbf{J} = 0.1$ and $\mathbf{p} = 0.1\mathbf{e}_z$. If the system were integrable, each phase space trajectory would be confined to a two-dimensional torus, and would appear in the figure as a densely dotted curve. Instead, the figure shows that the phase space contains chaotic regions, where trajectories ergodically visit three-dimensional volumes, as well as quasi-integrable regions, where trajectories are confined to two-dimensional tori.

III. QUANTUM HAMILTONIAN

The quantization of the classical Hamiltonian [Eq. (16)] is straightforward, and proceeds as in any standard angular momentum text (see, for instance, Ref. 4). There is only one subtlety. Since \mathbf{p}' and \mathbf{J}' have a nonvanishing Poisson bracket, their quantum counterparts do not commute, and the quantization of terms like $p'_\mu J'_\nu$ suffers from an ordering

ambiguity. We can sidestep this problem because we only need to quantize the components of $\Theta^{(2)}$: since $[J'_\mu, p'_\nu]_{\text{cl}}$ is $\mu\nu$ -antisymmetric, while each matrix $\hat{\mathcal{M}}_q^{(2)}$ is symmetric, the operators $\Theta_q^{(2)}$ are independent of the relative ordering of \mathbf{p}' and \mathbf{J}' . For the remainder of the paper, \mathbf{p} , \mathcal{H} , etc., will refer to the appropriate quantum operators (or their eigenvalues) unless otherwise noted.

Breaking the Hamiltonian down into \mathcal{H}_0 and $\delta\mathcal{H}$, respectively the first three and last two terms of Eq. (16), allows us to proceed perturbatively. Since $\delta\mathcal{H}$ vanishes for a free rigid rotor, this separates out the effects of the fluid. The $\mathbf{p} \cdot \mathbf{J}$ term also is absent for a free rotor, but this term commutes with p^2 and \mathcal{H}_{rr} , so it can be treated exactly.

Because \mathbf{p} is conserved, we can fix $\mathbf{p} = k\mathbf{e}_z$, $k \geq 0$, with no loss of generality. A convenient basis for the remaining (angular) degrees of freedom is the set of simultaneous eigenvectors of J^2 , J'_z , and J_z ; the eigenvector with respective eigenvalues $J(J+1)$, K , and M is denoted by $|JKM\rangle$. The tensor operators [Eq. (18)] become

$$\Pi_q^{(2)} = \frac{2}{\sqrt{6}}k^2\mathcal{D}_{0q}^{(2)}, \quad (19a)$$

$$\Theta_q^{(2)} = k \left(\frac{1}{2}J_- \mathcal{D}_{-1q}^{(2)} + \frac{2}{\sqrt{6}}J_z \mathcal{D}_{0q}^{(2)} - \frac{1}{2}J_+ \mathcal{D}_{1q}^{(2)} \right), \quad (19b)$$

where $J_\pm \equiv J_x \pm iJ_y$. Their matrix elements are expressible in terms of Wigner 3- j symbols:

$$\begin{aligned} \langle J_2 K_2 M_2 | \Pi_q^{(2)} | J_1 K_1 M_1 \rangle &= \frac{2}{\sqrt{6}}k^2(-1)^{K_1+M_1} \sqrt{(2J_2+1)(2J_1+1)} \times \\ &\quad \begin{pmatrix} J_2 & 2 & J_1 \\ K_2 & q & -K_1 \end{pmatrix} \begin{pmatrix} J_2 & 2 & J_1 \\ M_2 & 0 & -M_1 \end{pmatrix} \\ &= (-1)^{K_1} \begin{pmatrix} J_2 & 2 & J_1 \\ K_2 & q & -K_1 \end{pmatrix} \langle J_2 M_2 || \Pi^{(2)} || J_1 M_1 \rangle, \end{aligned} \quad (20a)$$

and

$$\begin{aligned} \langle J_2 K_2 M_2 | \Theta_q^{(2)} | J_1 K_1 M_1 \rangle &= k(-1)^{K_1+M_1} \sqrt{(2J_2+1)(2J_1+1)} \begin{pmatrix} J_2 & 2 & J_1 \\ K_2 & q & -K_1 \end{pmatrix} \times \\ &\quad \left\{ \frac{1}{2} \sqrt{(J_2-M_2)(J_2+M_2+1)} \begin{pmatrix} J_2 & 2 & J_1 \\ M_2+1 & -1 & -M_1 \end{pmatrix} + \frac{2}{\sqrt{6}}M_2 \begin{pmatrix} J_2 & 2 & J_1 \\ M_2 & 0 & -M_1 \end{pmatrix} - \right. \\ &\quad \left. \frac{1}{2} \sqrt{(J_2-M_2+1)(J_2+M_2)} \begin{pmatrix} J_2 & 2 & J_1 \\ M_2-1 & 1 & -M_1 \end{pmatrix} \right\} \\ &= (-1)^{K_1} \begin{pmatrix} J_2 & 2 & J_1 \\ K_2 & q & -K_1 \end{pmatrix} \langle J_2 M_2 || \Theta^{(2)} || J_1 M_1 \rangle. \end{aligned} \quad (20b)$$

The simple dependence of the matrix elements on K_1 , K_2 and q is a consequence of the tensorial nature of the operators, and is guaranteed by the Wigner-Eckart theorem. The reduced matrix elements vanish unless $M_2 = M_1$, by inspection, so J_z commutes with both \mathcal{H}_0 and $\delta\mathcal{H}$. This is to be expected from the classical conservation of $\mathbf{p} \cdot \mathbf{J}$, which equals kJ_z for our choice of \mathbf{p} .

The eigenvectors of \mathcal{H}_0 are the simultaneous eigenvectors of the rigid rotor Hamiltonian and J_z . Since \mathcal{H}_{rr} can be written in a normalized form,

$$\mathcal{H}_{rr}(A, B, C) = \frac{1}{2}(A+C)J^2 + \frac{1}{2}(A-C)\mathcal{H}_{rr}(1, \kappa, -1), \quad (21)$$

the eigenvectors depend only on the asymmetry parameter $\kappa = (-A + 2B - C)/(A - C)$. The eigenstates evolve continuously with κ ; they become eigenstates of J'_x and J'_z in the prolate ($\kappa \rightarrow -1$) and oblate ($\kappa \rightarrow 1$) limits respectively, with corresponding eigenvalues K_{-1} and K_{+1} . Following standard notation, we denote these states as $|\tau M\rangle$, where $\tau \in \{J_{K_{-1}K_{+1}}\} = \{0_{00}, 1_{01}, 1_{11}, 1_{10}, \dots\}$ indicates both the angular momentum and the two limiting values of K , and M is the eigenvalue of J_z . The unperturbed energies are

$$E_{\tau M}^{(0)} = \frac{1}{2}\alpha_0^{(0)}k^2 + \beta_0^{(0)}Mk + \frac{1}{2}(A+C)J(J+1) + \frac{1}{2}(A-C)\mathcal{E}_\tau(\kappa), \quad (22)$$

written in terms of the normalized rigid rotor eigenvalues $\mathcal{E}_\tau(\kappa)$.

We are now in a position to find the perturbed energies to any order in $\delta\mathcal{H}$. The expansion can be reordered as an expansion in the momentum k . The first-order correction comes from the diagonal elements of $\Theta^{(2)}$, which turn out to be proportional to M for each τ . A given level has energy

$$E_{\tau M}(k) = \frac{1}{2}(A + C)J(J + 1) + \frac{1}{2}(A - C)\mathcal{E}_{\tau}(\kappa) + \tilde{B}_{\tau}Mk + \frac{1}{2}\tilde{A}_{\tau M}k^2 + O(k^3), \quad (23)$$

where \tilde{B}_{τ} and $\tilde{A}_{\tau M}$ are to be calculated. Higher-order terms are suppressed by additional factors of $k\beta_q^{(2)}$ or $k^2\alpha_q^{(2)}$; for the cases we consider in the next Section, these factors are less than 10^{-3} , so it is reasonable to truncate the expansion here. Clearly $\tilde{A}_{\tau M}^{-1}$ is an effective mass; it reduces to the mass of the body in the absence of the fluid. The constant \tilde{B}_{τ} is a pseudoscalar associated with the family of levels $|\tau M\rangle$. It is nonzero only in the presence of the fluid, and only when the immersed body is *chiral*. Judging from the spectrum, \tilde{B}_{τ} measures the tendency of the immersed body to have its linear and angular momenta aligned. When this tendency is strong, the body behaves as a kind of “quantum propeller.”

IV. MOLECULAR SURFACE MODEL AND NUMERICAL RESULTS

In order to apply these results to a real system, we must specify the fluid density ρ_f , model the surface ∂V_0 and mass density $\rho(\mathbf{x})$ which characterize the immersed body, and calculate the tensors \hat{M} , \hat{G} , and \hat{I} from these inputs. In this section we consider the interesting case of an immersed *molecule* in superfluid helium. The fluid density ρ_f is approximately $0.1 \text{ amu}\cdot\text{\AA}^{-3}$. The mass density of the molecule can be represented as $\rho(\mathbf{x}) = \sum_i m_i \delta(\mathbf{x} - \mathbf{x}_i)$, where the atomic coordinates \mathbf{x}_i are known. Helium is kept away from the molecule primarily by the short-ranged Fermi repulsion between molecular electrons and helium electrons. This results in a smoothly varying helium density, interpolating from zero near the molecule to ρ_f far away. Our model approximates this smooth variation by a discontinuous jump, localized on the imaginary surface ∂V_0 . The optimal choice of surface is not obvious, but some criteria are clearly important. The surface should share the symmetries of the molecule; it should be smooth, since the electronic densities are smooth; and its size and shape should be physically reasonable: when compared to the actual helium density profile, the surface should approximate the surface $\rho = \frac{1}{2}\rho_f$. With these criteria in mind, we model the surface ∂V_0 for an immersed molecule in the following way. First, we place a sphere of radius R_i at each atomic coordinate \mathbf{x}_i . Each radius is proportional to the van der Waals distance between a helium atom and an atom of type i : $R_i = cR_{\text{He-}i}$, where the parameter c will be of order 1. (For our calculations, we used $R_{\text{He-H}} = 2.60 \text{ \AA}$, $R_{\text{He-F}} = 2.87 \text{ \AA}$, and $R_{\text{He-O}} = 2.92 \text{ \AA}$.) The union of these spheres forms a cuspy volume. The surface radius of the body volume, relative to an origin within the molecule, is represented in polar coordinates as $r_s(\theta, \phi)$. We then smooth the function r_s using the rotationally invariant linear operator which maps $Y_{lm}(\theta, \phi) \mapsto \exp(-\alpha l) Y_{lm}(\theta, \phi)$, with $\alpha = 0.1$, to yield the final surface ∂V_0 . This prescription gives a single-parameter family of smooth surfaces which share the symmetry of the molecule; the parameter c can be adjusted to exclude superfluid from an appropriately sized volume.

Once the surface is fixed, the fluid tensors can be calculated either numerically or analytically. We used a perturbative analytical method, valid for nearly spherical surfaces, where the surface radius is a weakly varying function of polar angle: $r_s(\theta, \phi) = r_0(1 + \epsilon(\theta, \phi))$, with $\epsilon \ll 1$. The fluid response functions ψ_{μ} and χ_{μ} (see Section II) can then be calculated as power series in ϵ , as can the fluid contributions to the tensors. This calculation has been carried through to second order, which is the lowest order at which nontrivial rotational-translational coupling (i.e. a nonzero value for \tilde{B}_{τ}) is seen. The calculation and results are described in the Appendix.

We present data for the low-lying levels of two different molecules: hydrogen peroxide (HOOH) and dioxygen difluoride (FOOF). These molecules are depicted in Fig. 2, with structural parameters taken from Ref. 6. Each has a C_2 point group, which we have taken to be $C_2(y)$ by an appropriate rotation of body axes. The allowed rotational levels all have the same parity under rotation by π around the y -axis: either even $(0_{00}, 1_{11}, 2_{02}, \dots)$ or odd $(1_{01}, 1_{10}, 2_{12}, \dots)$, depending on the symmetry of the joint electronic/nuclear wavefunction. In the case where allowed levels are odd, the $J = 0$ state is forbidden, so the ground state of the immersed molecule has $J = 1$, and, by Eq. (23), a nonzero linear momentum. The ground state momentum is $k_0 = |\tilde{B}_{\tau_0}/\tilde{A}_{\tau_0,+1}|$, where τ_0 is the ground state with $J = 1$.

The results for HOOH and FOOF are presented in Tables I and II respectively, in units where $\hbar = c = k_B = 1$. The surfaces considered can be parametrized by their mean radius r_0 , shown in the first column. The values displayed correspond to the parameter range $0.5 \leq c \leq 1.5$ for each molecule. Although the inverse effective masses $\tilde{A}_{\tau M}$ are level-dependent, this dependence is very weak, and $\tilde{A}_{\tau M} \approx \alpha_0^{(0)}$ for the tabulated cases. This approximate value is displayed, as \tilde{A} , in the second column. The remaining columns list the zero-momentum energies $E_{\tau}(0)$ and chiral splitting constants \tilde{B}_{τ} for the $C_2(y)$ -odd levels $\tau = 1_{01}$ and $\tau = 1_{10}$.

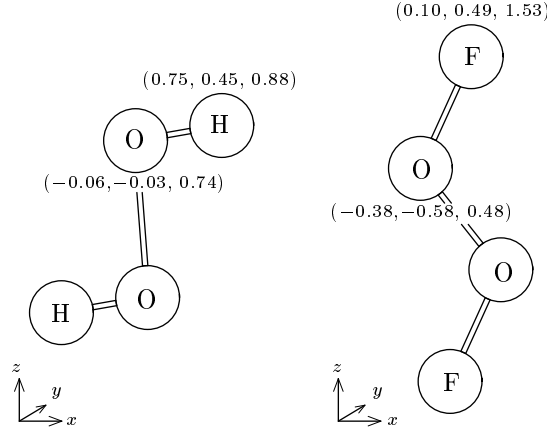


FIG. 2: Structures of the chiral molecules HOOH and FOOF. Atomic coordinates (x, y, z) are shown, in \AA , for two atoms in each molecule. The undisplayed coordinates are obtained from these by a symmetry transformation, $R_y(\pi) : (x, y, z) \mapsto (-x, y, -z)$.

TABLE I: Results for HOOH.

$r_0(\text{\AA})$	$\tilde{A}(\text{cm}^{-1}\text{-}\text{\AA}^2)$	$E_{1_{01}}(0)(\text{cm}^{-1})$	$\tilde{B}_{1_{01}}(\text{m}^{-1}\text{-}\text{\AA})$	$E_{1_{10}}(0)(\text{cm}^{-1})$	$\tilde{B}_{1_{10}}(\text{m}^{-1}\text{-}\text{\AA})$
1.86	5.91	10.3	-0.1	60.8	2.0
2.47	5.62	10.1	-0.1	56.2	2.5
3.06	5.23	9.87	-0.2	52.0	3.9
3.63	4.75	9.54	-0.3	48.6	5.1
4.21	4.22	9.15	-0.4	46.2	5.7
4.78	3.68	8.69	-0.3	44.8	5.4

To put the results in context, consider the physical parameters of current nanodroplet experiments, together with the hydrogen peroxide results. Ignoring finite-size effects, the thermal momentum distribution is expected to be Maxwellian, i.e. $dP/dk = Ck^2 \exp\left(-\frac{1}{2}\tilde{A}k^2/T\right)$. The nanodroplet temperature is $T = 0.4$ K, or 1.5 cm^{-1} in our units. This corresponds to a typical thermal momentum of $k_{rms} = 1 \text{ \AA}^{-1}$ for HOOH. The ground-state momentum k_0 , on the other hand, is only about 0.01 \AA^{-1} , and is completely overwhelmed by thermal fluctuations. The $\tau = 1_{01}$ and $\tau = 1_{10}$ energy levels will each acquire fine structure by splitting into three evenly spaced sublevels with different values of M ; we estimate the spacing for these two sets of sublevels to be $0.1 - 0.3 \text{ m}^{-1}$ and $2 - 5 \text{ m}^{-1}$ respectively. Moreover, the center level ($M = 0$) in each triplet is sharp, while the wings ($M = \pm 1$) are broadened by the thermal spread in momentum. Because the experimental linewidth for rotational transitions is small, on the order of 1 m^{-1} , we expect this fine structure to be resolvable in the $1_{01} \rightarrow 1_{10}$ absorption line for HOOH. This line should appear as a sharp central peak, with broader peaks symmetrically placed on either side, at $\pm 0.02 - 0.05 \text{ cm}^{-1}$.

More generally, the resolvable fine structure of the absorption line for a dipole transition $\tau_a \rightarrow \tau_b$ will depend on the relative values of $k\tilde{B}_a$, $k\tilde{B}_b$, and the natural linewidth Γ . There may be three peaks (if $k\tilde{B}_b \gg \Gamma \gg k\tilde{B}_b - k\tilde{B}_a$), $2J_a + 1$ peaks (if $k\tilde{B}_b - k\tilde{B}_a \gg \Gamma \gg k\tilde{B}_b$), $3(2J_a + 1)$ peaks (if $k\tilde{B}_b$ and $k\tilde{B}_b - k\tilde{B}_a \gg \Gamma$), or more complicated possibilities when some peaks overlap.

V. DISCUSSION

In this paper we have presented a classical model for the behavior of a molecule immersed in superfluid; and we have shown that the quantized version of the model has interesting features which should be, under certain conditions, spectroscopically detectable. In particular, chiral molecules can act as “quantum propellers,” coupling linear and angular momenta via their interaction with the superfluid medium, and this leads to a characteristic splitting of spectral lines. Our model simplifies the superfluid dynamics greatly, which presumably affects the quantitative accuracy of our results. We will conclude by discussing possible remedies for the shortcomings of our model.

One important physical effect that we have ignored is the formation of structured shells of helium atoms around a

TABLE II: Results for FOOF.

$r_0(\text{\AA})$	$\tilde{A}(\text{cm}^{-1}\text{-}\text{\AA}^2)$	$E_{1_{01}}(0)(\text{cm}^{-1})$	$\tilde{B}_{1_{01}}(\text{m}^{-1}\text{-}\text{\AA})$	$E_{1_{10}}(0)(\text{cm}^{-1})$	$\tilde{B}_{1_{10}}(\text{m}^{-1}\text{-}\text{\AA})$
1.97	2.91	1.92	0.2	5.19	-0.3
2.68	2.63	1.82	0.1	2.25	-0.1
3.32	2.69	1.86	0.1	5.10	-0.4
3.93	2.53	1.82	0.1	5.02	-0.4
4.53	2.33	1.77	0.1	4.93	-0.4
5.13	2.13	1.71	0.1	4.81	-0.4

solvated impurity, which leads to a nonuniform fluid density. The model can be naturally extended to include this, by allowing the fluid density ρ_f to vary spatially, while maintaining a time-independent profile in the body frame. This approach has been used by other authors to estimate the superfluid-induced increase in the moments of inertia of linear or highly symmetric molecules.^{7,8} The effect of a nonuniform density can be dramatic. For instance, SF_6 has $I = 180 \text{ amu}\text{-}\text{\AA}^2$ in vacuum, which increases by $\Delta I = 310 \text{ amu}\text{-}\text{\AA}^2$ when the molecule is immersed in a helium droplet. The model presented here gives $\Delta I < 25 \text{ amu}\text{-}\text{\AA}^2$, an order of magnitude too small. By contrast, a calculation using a nonuniform density predicts $\Delta I = 170 \text{ amu}\text{-}\text{\AA}^2$, which is more than half of the experimental value.⁸ The comparison demonstrates that a rigid body with solvation shells attached drags more mass when it moves than one without them. It is tempting to speculate that the calculated chiral splitting constants \tilde{B}_τ will also increase when a nonuniform density is allowed; but this may not be the case, for two reasons. First, because the off-diagonal Hamiltonian matrix $\hat{\beta} = -\hat{M}^{-1}\hat{G}\hat{I}^{-1}$ to lowest order in \hat{G} , increases in the rotational-translational coupling tensor are counteracted by corresponding increases in the hydrodynamic mass and inertia tensors. Second, because attaching solvation shells to the immersed body simply builds a larger rigid body, to some extent, and the constants \tilde{B}_τ always vanish for a rigid body. Therefore, while allowing a nonuniform fluid density may alter our results, it is difficult to predict the outcome without performing a full calculation.

Microscopic details of the superfluid structure are also neglected by a continuum hydrodynamic approach. These details are better treated by path-integral and diffusion Monte Carlo methods, which have proven successful in predicting the rotational constants of immersed molecules.⁷ It is likely that the hydrodynamic mass and rotational-translational tensors described here can also be extracted from such calculations, and this information would be a useful complement to the hydrodynamic results. Monte Carlo methods could also be used to address another neglected phenomenon: the quantum-mechanical tunnelling between left-handed and right-handed forms of a chiral molecule. This may play a pronounced role in hydrogen peroxide, where the torsional ground state (a symmetric superposition of left- and right-handed forms) is 11 cm^{-1} below the first (antisymmetric) excited state.⁹ Because the splitting is so large, comparable even to the rotational level spacing, the enantiomers are strongly mixed, making questionable our rigid-body treatment of the molecule. We expect the surrounding superfluid to suppress tunnelling, but a detailed calculation, without the assumption of rigidity, is needed for a quantitative assessment. The main difficulty in applying Monte Carlo methods would be finite-size effects: since translational symmetry is strongly broken in small droplets, while rotational symmetry is preserved, the finite-size corrections to \hat{M} and \hat{G} are presumably more drastic than those to \hat{I} . A number of other microscopic techniques have been applied to molecular impurities in superfluid droplets (see Ref. 7 for a recent review), such as density functional theory, and these more elaborate methods may also be applicable to the phenomena we have described.

Finally, experimental data would be extraordinarily useful in refining the current model. The spectroscopic signatures we have described should be present for any chiral molecule, but not all candidate molecules will have the large splitting constants necessary to resolve the fine structure. Nanodroplet experiments have been conducted using many different species of impurity molecule; Ref. 3 contains an exhaustive list. However, almost none of the studied molecules are chiral, so it is not surprising that no quantum propeller has yet been seen. We have suggested hydrogen peroxide (HOOH) as one strong candidate. Ideally, the present paper will provide sufficient impetus for more detailed investigations, both theoretical and experimental.

Acknowledgments

This work was funded by a Department of Education GAANN Fellowship, No. P200A970615.

*

APPENDIX A: CALCULATION OF FLUID TENSORS

For approximately spherical surfaces, it is possible to calculate the hydrodynamic mass, rotational-translational coupling, and inertia tensors as perturbation series in the deviation from sphericity. Consider a surface at $r_s(\theta, \phi) = r_0(1 + \epsilon(\theta, \phi))$. The surface normal times the area element is

$$\frac{\mathbf{n} da}{r_0^2 d^2 \Omega} = (1 + \epsilon) (\mathbf{e}_r + i (\mathbf{e}_r \times \mathbf{J})) (1 + \epsilon), \quad (\text{A1})$$

where

$$\mathbf{J} \equiv i \mathbf{e}_\theta \frac{1}{\sin \theta} \frac{\partial}{\partial \phi} - i \mathbf{e}_\phi \frac{\partial}{\partial \theta} \quad (\text{A2})$$

is the usual vector of first-order differential operators on the sphere. For any scalar function ϕ ,

$$\nabla \phi \cdot \frac{\mathbf{n} da}{r_0^2 d^2 \Omega} = (1 + \epsilon)^2 \frac{\partial \phi}{\partial r} + \frac{1}{r_0} \mathbf{J} \phi \cdot \mathbf{J} \epsilon, \quad (\text{A3})$$

with derivatives evaluated at $r = r_s$. Applying this to Eq. (5a) for the translational response function ψ_μ yields

$$\frac{\partial \psi_\mu}{\partial r} = n_\mu - \frac{1}{r_0(1 + \epsilon)^2} \mathbf{J} \psi_\mu \cdot \mathbf{J} \epsilon + \frac{1}{1 + \epsilon} i \epsilon_{\mu\nu\lambda} n_\nu (\mathbf{J} \epsilon)_\lambda, \quad (\text{A4})$$

where $n_\mu = \mathbf{e}_\mu \cdot \mathbf{e}_r$, and with derivatives evaluated at $r = r_s$. If ψ_μ is expanded in orders of ϵ , as $\psi_\mu = \psi_\mu^{(0)} + \psi_\mu^{(1)} + \dots$, and functions evaluated at r_s are expanded in Taylor series around r_0 , then Eq. (A4) gives a single equation at each order in ϵ :

$$\frac{\partial \psi_\mu^{(0)}}{\partial r} = n_\mu, \quad (\text{A5a})$$

$$\frac{\partial \psi_\mu^{(1)}}{\partial r} + r_0 \epsilon \frac{\partial^2 \psi_\mu^{(0)}}{\partial r^2} = -\frac{1}{r_0} \mathbf{J} \psi_\mu^{(0)} \cdot \mathbf{J} \epsilon + i \epsilon_{\mu\nu\lambda} n_\nu (\mathbf{J} \epsilon)_\lambda, \quad (\text{A5b})$$

and so forth, where now all derivatives are evaluated at $r = r_0$. Moreover, $\nabla^2 \psi_\mu^{(n)} = 0$ and $|\nabla \psi_\mu^{(n)}(\mathbf{x})| \rightarrow 0$ as $|\mathbf{x}| \rightarrow \infty$ for each n . The zeroth-order equation can be solved for $\psi_\mu^{(0)}$, and in general the equation of order ϵ^n can be solved for $\psi_\mu^{(n)}$ once all the $\psi_\mu^{(m)}$ with $m < n$ are known. Therefore ψ_μ can be calculated to any order in ϵ , though the process rapidly becomes tedious. Similarly, the rotational response function χ_μ satisfies the simpler equation

$$\frac{\partial \chi_\mu}{\partial r} = -i r_0 (\mathbf{J} \epsilon)_\mu - \frac{1}{r_0(1 + \epsilon)^2} \mathbf{J} \chi_\mu \cdot \mathbf{J} \epsilon \quad (\text{A6})$$

at $r = r_s$, which follows from Eq. (5b); and this can be used to find χ_μ to any order in ϵ , in exactly the same way.

Once the response functions are in hand, Eqs. (10) can be evaluated to obtain the fluid tensors. This, too, is done order-by-order in ϵ . The results are best expressed as angular averages. Through second order in ϵ ,

$$\frac{\delta M_{\mu\nu}}{4\pi \rho_f r_0^3} = \frac{1}{6} \delta_{\mu\nu} + \left\langle \left(-\frac{9}{4} n_\mu n_\nu + \frac{5}{4} \delta_{\mu\nu} \right) \epsilon \right\rangle - \left\langle \psi_\mu^{(1)} \frac{\partial \psi_\nu^{(1)}}{\partial r} \right\rangle, \quad (\text{A7a})$$

$$\frac{\delta G_{\mu\nu}}{4\pi \rho_f r_0^4} = \frac{1}{2} \epsilon_{\mu\nu\lambda} \langle n_\lambda \epsilon \rangle - \left\langle \psi_\mu^{(1)} \frac{\partial \chi_\nu^{(1)}}{\partial r} \right\rangle, \quad (\text{A7b})$$

$$\frac{\delta I_{\mu\nu}}{4\pi \rho_f r_0^5} = - \left\langle \chi_\mu^{(1)} \frac{\partial \chi_\nu^{(1)}}{\partial r} \right\rangle, \quad (\text{A7c})$$

where $\langle f \rangle \equiv \frac{1}{4\pi} \int f(\Omega) d^2 \Omega$, and functions are evaluated at r_0 . Here the first-order fields $\psi_\mu^{(1)}$ and $\chi_\mu^{(1)}$ are determined by their radial derivatives at r_0 , which are

$$\begin{aligned} \frac{\partial \psi_\mu^{(1)}}{\partial r} &= -\frac{3}{2} i \epsilon_{\mu\nu\lambda} n_\nu (\mathbf{J} \epsilon)_\lambda - 3 n_\mu \epsilon, \\ \frac{\partial \chi_\mu^{(1)}}{\partial r} &= -i (\mathbf{J} \epsilon)_\mu. \end{aligned} \quad (\text{A8})$$

Note that $\delta\hat{G}$ is antisymmetric to first order. Because the antisymmetric part of \hat{G} is eliminated by the correct choice of body origin, it was necessary to carry the calculation of $\delta\hat{G}$ to second order to obtain nontrivial rotational-translational coupling.

-
- ¹ S. Grebenev, B. Sartakov, J. P. Toennies, and A. F. Vilesov, *Science* **289**, 1532 (2000).
 - ² S. Grebenev, M. Havenith, F. Madeja, J. P. Toennies, and A. F. Vilesov, *J. Chem. Phys.* **113**, 9060 (2000).
 - ³ C. Callegari, K. K. Lehmann, R. Schmied, and G. Scoles, physics/0109070.
 - ⁴ D. M. Brink and G. R. Satchler, *Angular Momentum* (Clarendon Press, Oxford, 1993), 3rd ed.
 - ⁵ A. Bondi, *J. Phys. Chem.* **68**, 441 (1964).
 - ⁶ R. H. Jackson, *J. Chem. Soc.* p. 4585 (1962).
 - ⁷ Y. Kwon, P. Huang, M. V. Patel, D. Blume, and K. B. Whaley, *J. Chem. Phys.* **113**, 6469 (2000).
 - ⁸ K. K. Lehmann and C. Callegari, physics/0109009.
 - ⁹ P. Helminger, W. Bowman, and F. De Lucia, *J. Mol. Spectrosc.* **171**, 91 (1981).